

# Polymeric Layered Films for TiO<sub>2</sub>-Au/CuS Tandem Photothermal Catalytic H<sub>2</sub> Production in Harsh Seawater and Waste Plastic Media

Minmin Gao, Tianxi Zhang, Serene Wen Ling Ng, Wanheng Lu, Guo Tian, Wei Li Ong, Sergey M. Kozlov, and Ghim Wei Ho\*

Conventional suspension photocatalysts face stability and efficiency challenges in harsh, unconditioned environments characterized by high alkalinity, salinity, and organic species in seawater and wastewater. Moreover, suspension-based photothermal-assisted catalysis presents further challenges, particularly concerning formation of heterojunctions between photocatalysts and photothermal materials that disrupt charge-transfer pathways and are exacerbated by photothermal heating-induced carrier recombination. Here, a photocatalytic system is proposed in which three key photoprocesses: photothermal, photogeneration-charge separation, and photoredox are spatially decoupled yet coordinated, aimed at addressing prevalent challenges of photothermal-assisted catalysis and adsorption-mediated catalyst deactivation in harsh environments. Essentially, the proposed polymeric tandem photothermal catalytic (PTPC) film consists of TiO<sub>2</sub>/Au photocatalytic and CuS photothermal layers, spatially separated and encapsulated by polymeric layers, which serve as spacer inhibitors to conflicting photochemical-photothermal pathways and corrosion-resistant redox medium. The PTPC film exhibits enhanced light absorption, mass transfer, and photothermal effect, surpassing traditional suspension catalysts and enabling interfacial redox reactions on the passive film surface. The PTPC system represents a new paradigm of polymeric film photocatalysis, enabling unimpeded photoredox-photothermal pathways and catalyst stability for application in hostile seawater and plastic waste environments. Such a paradigm can be used to develop localized, onsite solutions for photothermal H<sub>2</sub> production that minimize logistical and environmental challenges.

## 1. Introduction

Over the past decades, most photocatalytic H<sub>2</sub> production systems are typically focused on suspension systems, where catalyst powders are dispersed in the reactive medium.<sup>[1–3]</sup> However, the configuration of suspension system faces challenges of light scattering by the photocatalyst and water, limited light penetration depth, sedimentation and agglomeration as well as insufficient mass transfer issues (Figure 1a).<sup>[4,5]</sup> Moreover, particulate suspension photocatalysts encounter stability and efficiency challenges in unconditioned, harsh environments such as those with high alkalinity, salinity, organic compounds, and sediments typical of seawater and wastewater.<sup>[6–9]</sup>

Besides, the traditional photocatalyst design is prevalently dominated by UV-light responsive materials, by virtue of the wide bandgap, highly active charge carriers, and a high redox potential.<sup>[10,11]</sup> Different strategies are proposed to broaden the utilization range of solar energy and maximize the solar-to-chemical energy conversion efficiency.<sup>[12–14]</sup> More recently, the photothermal effect has been effectively utilized to fully

M. Gao, T. Zhang, S. W. L. Ng, W. Lu, G. Tian, W. L. Ong, G. W. Ho  
Department of Electrical and Computer Engineering  
National University of Singapore  
Singapore 117583, Singapore  
E-mail: elehgw@nus.edu.sg

M. Gao, G. W. Ho  
Department of Materials Science and Engineering  
National University of Singapore  
Singapore 117575, Singapore  
S. M. Kozlov  
Department of Chemical and Biomolecular Engineering  
National University of Singapore  
Singapore 119260, Singapore

 The ORCID identification number(s) for the author(s) of this article can be found under <https://doi.org/10.1002/aenm.202404198>

© 2025 The Author(s). Advanced Energy Materials published by Wiley-VCH GmbH. This is an open access article under the terms of the [Creative Commons Attribution-NonCommercial](#) License, which permits use, distribution and reproduction in any medium, provided the original work is properly cited and is not used for commercial purposes.

DOI: 10.1002/aenm.202404198

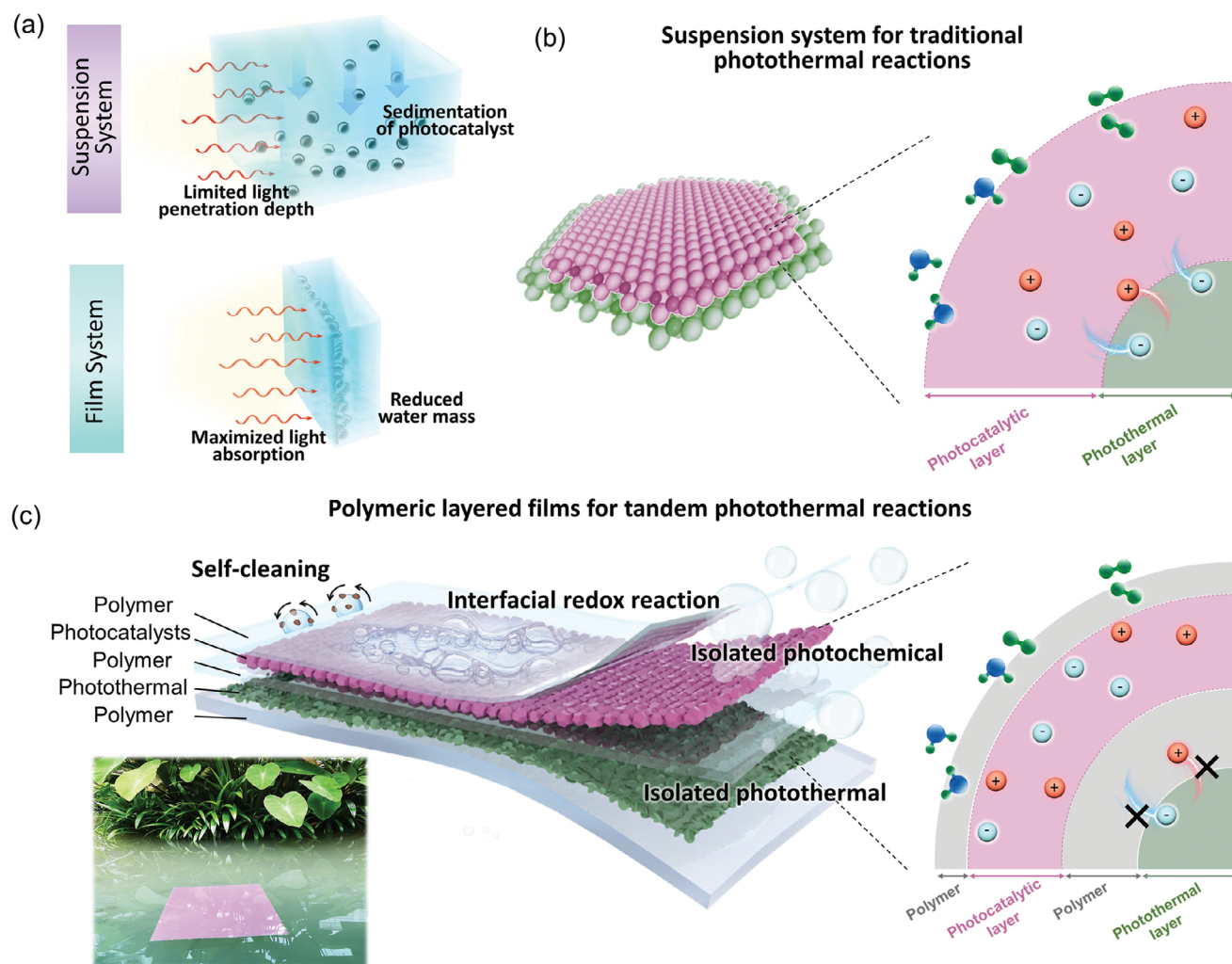


**Figure 1.** Schematic drawing of a) comparison between the traditional suspension system and film system. b) Suspension system for traditional photothermal reactions. c) The conceived flexible polymeric tandem photothermal catalytic (PTPC) film with cohesive photothermal and photochemical effects for  $H_2$  production from seawater and plastic waste.

harvest visible-NIR light and promote the catalysis activity through significant photoheating.<sup>[15,16]</sup> This photothermal effect will collectively improve the photocatalytic reactivity, through enhanced charge carriers' mobility, Gibbs free energy, mass transfer of reactants, and release of produced  $H_2$  gas.<sup>[17–20]</sup> Nonetheless, when photothermal materials are incorporated into photocatalysts, they form heterojunctions potentially interfering with the charge transfer pathway which could either enhance or detract from the overall catalytic efficiency, depending on the flow of charge carriers' passageway (Figure 1b). Additionally, photothermal heating might conversely promote the recombination of charge carriers, negatively impacting the photochemical reactivity and overall catalytic performance.<sup>[21,22]</sup> Moreover, photothermal catalysis in suspension systems frequently encounters catalyst deactivation challenges, stemming from a combination of chemical, thermal, and mechanical mechanisms inherent in harsh, unconditioned environments. Chemically, catalyst poisoning occurs through chemisorption of deleterious species, intermediates, etc. on catalytic sites. Thermally, the photother-

mal effects can lead to deactivation through active phase-support reactions or crystallite growth, and mechanically, harsh conditions may cause a loss of surface area and the collapse/blockage of the catalyst's nanostructure or pores. Each of these catalyst deactivation mechanisms drastically reduces the viability of accessible active sites, posing significant hurdles that must be addressed to harness the full potential of photothermal-mediated catalysis. Notably, it is also challenging to reap the benefits of the photothermal effect in a suspension system as the localized heat is unable to achieve a confined hot zone and instead inevitably dissipates into the bulk liquid.<sup>[23]</sup> Moreover, the configuration of the suspension system necessitates that light passes through the bulk water medium before reaching the surface of photothermal materials, which significantly diminishes the amount of adsorbed light, the temperature increase, and the catalytic activity of these materials.<sup>[4]</sup> The presented complexities in photothermal-mediated photocatalysis can be addressed through the design of innovative photocatalytic systems that function effectively in dynamic, unstructured water environments,<sup>[24,25]</sup>

yet such developments remain undemonstrated to date.

Here, we introduce a spatially decoupled, polymeric passivated catalytic system designed to facilitate pivotal photoprocesses such as photothermal, photogeneration-charge separation, and redox at distinct locations. This polymeric layered scheme effectively mitigates charge transfer interference between the photothermal materials and co-catalysts, while also shielding against adsorption-induced catalyst deactivation. The proposed system features a polymeric tandem photothermal catalytic (PTPC) film, which integrates a photocatalytic  $\text{TiO}_2/\text{Au}$  with a photothermal CuS, separated by polydimethylsiloxane (PDMS) layers immobilized on top and bottom of the film, and between the photocatalytic and photothermal layers (Figure 1c). The introduction of an intermediary PDMS layer achieves spatial separation between the photocatalytic and the photothermal layers, inhibiting cross-interference in charge transfer and simultaneously mediating confined photoheating. PDMS was selected for the tandem-layered photothermal catalytic films due to its transparency in the visible and NIR spectra, which maximizes light absorption by the photothermal material. Additionally, it is chemically and thermally stable for photocatalytic purposes, possesses excellent extensibility for flexibility and conformal usage, and is hydrophobic, enabling a self-cleaning function. Meanwhile, the encapsulating PDMS layer serves as a reaction medium for the photocatalyst, boosting its tolerance to harsh environments. This, in turn, prevents the deactivation of active sites, which typically results from diverse adsorption phenomena, thereby prolonging catalyst life. The observed interfacial redox reactions on the PDMS surface are verified by Kelvin Probe Force Microscopy (KPFM), photovoltage measurements, in-situ electron paramagnetic resonance (EPR), and simulations. The PTPC film demonstrates enhanced light absorption, and photothermal effects, and features self-cleaning surfaces, outperforming traditional suspension catalysts in the stable  $\text{H}_2$  production from challenging water sources such as seawater and plastic waste. This work introduces a pioneering approach in employing polymeric layered films to optimize light and photoheat harvesting for tandem photothermal catalysis in bulk, challenging water environments. It potentially allows for precise and independent management of the typically conflicting photoredox and photothermal functions. The PTPC system significantly improves the practicality of photocatalysis in harsh water, thereby extending its sustainability and durability, and promises onsite solutions for  $\text{H}_2$  production that reduce environmental and logistical burdens.

## 2. Results and Discussion

The flexible PTPC film is designed for spatially decoupled photothermal and photochemical  $\text{H}_2$  production as shown in Figure 1c. The photothermal effect is well-acknowledged for its ability to boost photocatalytic activity due to the temperature rise of the photocatalyst locally. Nevertheless, direct contact between the photocatalyst semiconductor ( $\text{TiO}_2$ ) and the photothermal semiconductor (CuS) may form Type-I heterojunction, potentially lowering the reduction capability of  $\text{TiO}_2$  (Figure S1, Supporting Information). When both the semiconductor ( $\text{TiO}_2$ ) and photothermal material (CuS) are simultaneously excited, competition arises between the recombination of electron holes and the

photothermal effect of CuS. On one hand, the photothermal effect of CuS could favor the photocatalytic reaction. On the other hand, the electrons from Au may recombine with the holes on CuS, further reducing the concentration of efficient electrons and undermining the overall photocatalytic performance. This is further complicated by the photothermal effect of CuS, which can elevate the local temperature, expediting the recombination of UV-generated electron-hole pairs in  $\text{TiO}_2$ . The conundrum between charge transfer separation and photothermal in catalysis revolves around the intricate balance and interactions between photothermal effects, charge transfer pathways, and their mutual influence on catalytic efficiency. Within the PTPC system, light and photoheat absorption can be maximized while sanctioning isolated photoredox and photothermal processes, which might otherwise conflict. The PTPC system significantly enhances the viability of photocatalysis in challenging water conditions, thus advancing its sustainability and reliability.

In Figure 1c, the flexible PTPC film is vertically structured with each layer playing a distinctive role.  $\text{TiO}_2/\text{Au}$  serve as the photocatalytic layer, with  $\text{TiO}_2$  as the photoactive material and Au nanoparticles as the cocatalyst for enhanced charge transfer in photochemical  $\text{H}_2$  production. CuS plays the essential role of a photothermal layer to extend the light absorption to Vis-NIR range and convert the absorbed energy to heat for photothermal-assisted  $\text{H}_2$  production. These functional layers are further assembled with a top and bottom PDMS encapsulation to form a flexible film architecture beneficial for light absorption, water mass transfer,  $\text{H}_2$  gas release, and spatially decoupled photothermal and photochemical effects for  $\text{H}_2$  production. Additionally, the hydrophobic characteristics of PDMS layer will further endow self-cleaning properties, allowing contaminants adhering to the film surface to be readily cleansed.

The topography mapping image of PTPC film shows the continuous film structure of  $\text{TiO}_2/\text{Au}$  after coating with PDMS (Figure S2, Supporting Information). Due to the excellent extensibility of PDMS polymer, the PTPC film possesses the advantages of being stretchable, flexible, and conformable. Even when stretched, twisted, bent, or folded, the film retains its original shape once the applied external force is removed (Figure 2a–d). Noticeably, the PTPC film is highly conformable, seamlessly fitting onto the leaf (Figure 2e). The film can also be customized into arbitrary shapes and sizes depending on specific usage requirements (Figure S3, Supporting Information). For instance, the film can be shaped as an “artificial leaf” and simulate the natural photosynthesis for  $\text{H}_2$  generation under light irradiation (the inset in Figure 2f). These features enable easy adaptation while maintaining resilience against external forces, potentially expanding its scope of applications.

The cross-sectional scanning electron microscope (SEM) image of the PTPC film reveals a multilayered sandwich structure (Figure 2g). Elemental distribution along the PTPC film cross-section, depicted in the line scan delineates the layered structure of PDMS,  $\text{TiO}_2/\text{Au}$  photocatalytic, and CuS photothermal layer (Figure S4, Supporting Information). The photocatalytic layer reveals an average diameter of 4 nm Au nanoparticle (NP) distributed among  $\text{TiO}_2$  NP, confirmed by transmission electron microscope (TEM) (Figure 2h; Figure S5, Supporting Information). The lattice spacing of 0.32 and 0.35 nm corresponds to (110) and (101) planes of  $\text{TiO}_2$ , respectively, while the

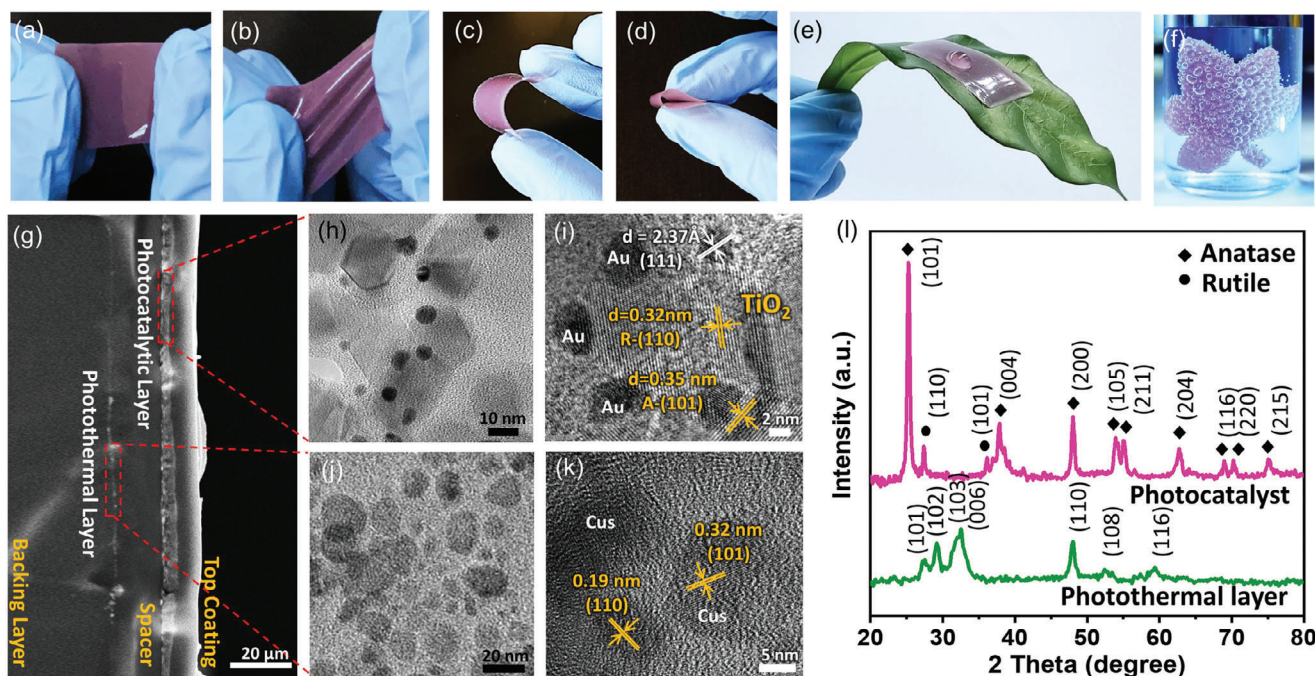


**Figure 2.** a–d) The excellent flexibility (stretching, twisting, bending, and folding) of PTPC film (the film size is 1.0 cm<sup>2</sup> × 1.5 cm). e) The conformability of PTPC film. f) The produced H<sub>2</sub> bubbles on the surface of tailored artificial leaves under light irradiation. g) SEM image of a cross-section view of PTPC. h) Low and i) high resolution TEM image of the photocatalytic layer TiO<sub>2</sub>/Au. j) Low and k) high resolution TEM image of the photothermal layer CuS. l) XRD pattern of the photocatalyst (TiO<sub>2</sub>/Au) and photothermal layer (CuS).

interplanar distance of 0.24 nm corresponds to (111) crystal facet of Au (Figure 2i).<sup>[26,27]</sup> CuS is chosen for its cost-effectiveness, low toxicity, and tunable photothermal properties, making it a highly promising photothermal material.<sup>[28,29]</sup> The presence of CuS in the photothermal layer is affirmed by the TEM image in Figure 2j. The high-resolution TEM image (Figure 2k) reveals lattice fringes of 0.19 and 0.32 nm, well indexed to (110) and (101) planes of CuS. To confirm the composition of the PTPC film, X-ray powder diffraction (XRD) characterization was performed. As shown in Figure 2l, the XRD pattern of the photocatalytic layer shows the presence of TiO<sub>2</sub> in the anatase and rutile phases with negligible Au peaks due to the relatively low Au loading. For the photothermal layer, the peaks correspond well to CuS (PDF Card No. 06–0464).

The flexible PTPC film offers additional advantages in optical absorption and thermal management for photothermal-assisted catalysis. Unlike typical suspension systems, where light must traverse bulk water to reach the catalyst surface, encountering scattering and sedimentation issues that further deteriorate light penetration (Figure 1a), the PTPC film only requires light to penetrate through its thickness in the order of tens of microns. This design ensures optimal light irradiation area. Furthermore, compared to suspension systems, the film requires reduced water volume, thus enhancing the efficiency of bulk water photothermal heating. Consequently, when an optimal amount of 8% Au was loaded (Figure S6, Supporting Information), the TiO<sub>2</sub>/Au with a PDMS film exhibits an H<sub>2</sub> production activity superior to that of suspension system with stirring, maintaining a consistent H<sub>2</sub> generation rate of 120 mmol m<sup>-2</sup> h<sup>-1</sup> for 5 cycling tests (Figure 3a). Conversely, the suspension system without stir-

ring experiences a dramatic drop in H<sub>2</sub> generation from 110 to merely 24 mmol m<sup>-2</sup> h<sup>-1</sup> after 5 cycles. UV-vis absorption spectra of the unstirred photocatalyst suspension show a notable decline in light absorption over time, indicating a serious sedimentation issue of the photocatalyst (Figure S7, Supporting Information). This underscores the necessity of mechanical agitation in suspension systems to overcome the challenges of insufficient light absorption and photocatalyst settling. However, employing mechanical agitation is impractical for scaled-up applications. The PTPC system is designed to address the critical challenges inherent in suspension systems, achieving higher efficiency without the need for stirring and facilitating catalyst recycling, making it ideal for practical applications.

Apart from the desired light absorption, the PTPC system also enhances the photothermal effect, effectively utilizing photo-heat for photothermal-assisted catalytic reaction. As shown in Figure 3b, pure PDMS shows negligible light absorption across the spectrum. Due to the transparency of PDMS, TiO<sub>2</sub>/Au catalyst and TiO<sub>2</sub>/Au catalyst coated with a PDMS film exhibit similar light absorption with the LSPR peak of Au observed ≈530 nm.<sup>[30,31]</sup> Upon introducing photothermal material CuS, the PTPC shows a broad light absorption from UV to visible light, ascribed to the excellent light-harvesting capacity of CuS. Nonetheless, the direct introduction of CuS photothermal material into TiO<sub>2</sub>/Au photocatalyst in a suspension system disrupts the photochemical charge transfer pathway and photothermal heating, as evidenced by the apparent decline in H<sub>2</sub> production performance in Figure 3c. In a suspension system, TiO<sub>2</sub>/Au catalyst shows an average H<sub>2</sub> production rate of 110 mmol m<sup>-2</sup> h<sup>-1</sup> under UV light irradiation and slightly increased by 37% to

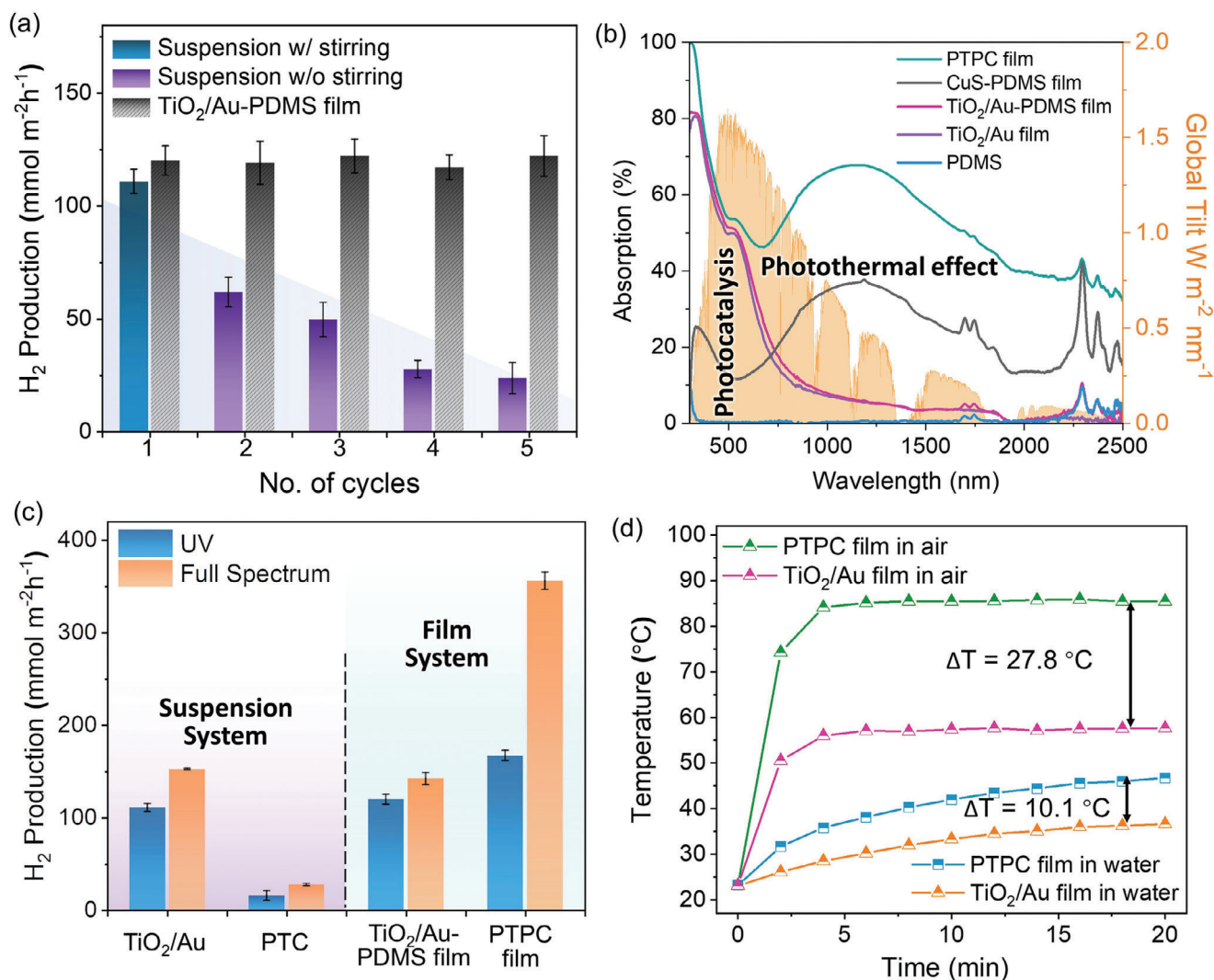


**Figure 3.** a) The comparison of H<sub>2</sub> evolution activity for a suspension system with/without stirring and TiO<sub>2</sub>/Au-PDMS film system. b) Absorption spectra of PDMS, TiO<sub>2</sub>/Au film, TiO<sub>2</sub>/Au-PDMS film, CuS-PDMS film, PTPC film, and spectral solar irradiance (AM 1.5). c) H<sub>2</sub> evolution activity of suspension system of TiO<sub>2</sub>/Au photocatalyst and TiO<sub>2</sub>/Au/CuS mixed catalyst (labeled as PTC), and film system of TiO<sub>2</sub>/Au-PDMS film and the PTPC film under UV and full spectrum irradiation. d) Temperature profiles of TiO<sub>2</sub>/Au film and PTPC film in air and water, respectively.

154 mmol m<sup>-2</sup> h<sup>-1</sup> under full spectrum. In contrast, an H<sub>2</sub> production rate of TiO<sub>2</sub>/Au/CuS catalyst decreases dramatically (by 86% under UV and 82% under full spectrum) when CuS is directly mixed with TiO<sub>2</sub>/Au catalyst in a suspension system. When the intermediary PDMS layer is intercalated between the photocatalytic and the photothermal layers, the PTPC achieves a significantly enhanced H<sub>2</sub> generation rate of 356 mmol m<sup>-2</sup> h<sup>-1</sup> under full spectrum, a 113% improvement compared to the TiO<sub>2</sub>/Au-PDMS film. Moreover, TiO<sub>2</sub>/Au catalyst coated with a PDMS film showed a similar H<sub>2</sub> production activity to that of TiO<sub>2</sub>/Au catalyst in suspension system. This stark contrast is associated with effective photothermal confinement and minimized interference of photothermal material with photochemical charge transfer separation. The infrared image reflects an elevated temperature within the PTPC film (Figure S8, Supporting Information) with a temperature difference of 27.8 °C in air and 10.1 °C in water compared to the TiO<sub>2</sub>/Au film (Figure 3d) which validates the

photothermal effect of CuS. Moreover, the contact angle of the coated PDMS layer remains consistent after continuous UV irradiation (Figure S9, Supporting Information), confirming the stability of the PTPC film. It is worth considering that the Si-H bond on the PDMS surface may possibly decompose and contribute to H<sub>2</sub> generation. Hence, this phenomenon was investigated and excluded to ensure a true H<sub>2</sub> production capacity of PTPC (Figures S10 and S11, Supporting Information).

The incorporation of PDMS layer is crucial to the distinctive design of the PTPC film-type system. The intrinsic characteristic of PDMS for charge induction and trapping extends the decay of charge carriers,<sup>[32]</sup> thereby enhancing charge density. To validate the presence of induced charges on the PDMS surface, photocurrent response and Kelvin probe force microscopy (KPFM) were performed to investigate surface potential and surface photovoltage.<sup>[33,34]</sup> Shielding half of the prepared TiO<sub>2</sub>/Au catalyst coated with top and bottom PDMS layers while

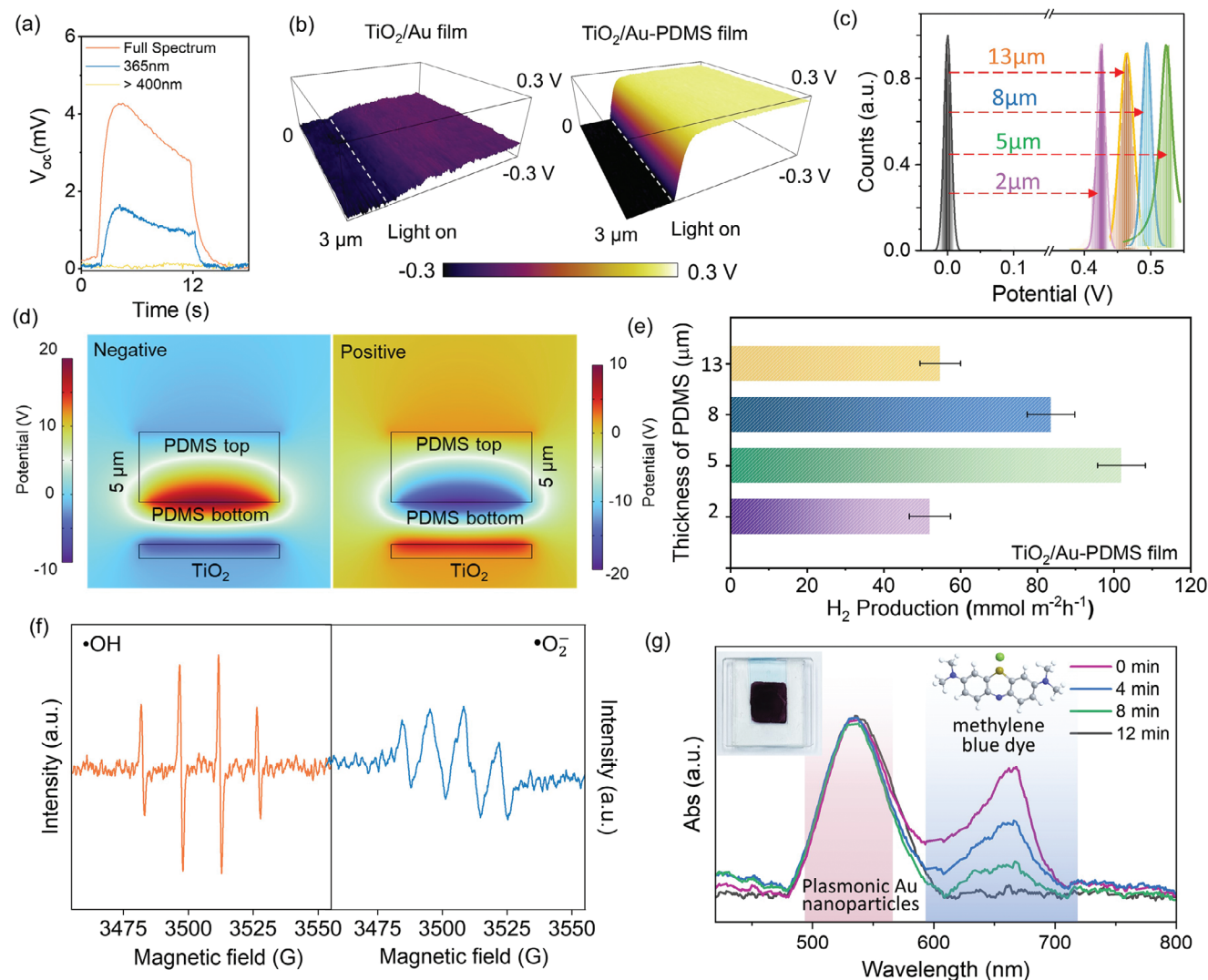


**Figure 4.** a) The photovoltages of  $\text{TiO}_2/\text{Au}$ -PDMS layer under 365 nm, visible light, and full spectrum irradiation. b) Surface potentials mapping of  $\text{TiO}_2/\text{Au}$  film and  $\text{TiO}_2/\text{Au}$ -PDMS film. c) Contact potential difference (CPD) profiles of  $\text{TiO}_2/\text{Au}$ -PDMS films with different PDMS layer thickness. d) COMSOL Multiphysics simulation results about the potential on the top of PDMS induced by the  $\text{TiO}_2$ . e) Average  $\text{H}_2$  production rate of  $\text{TiO}_2/\text{Au}$ -PDMS films with different PDMS layer thickness. f) EPR signals of  $\bullet\text{OH}$  and  $\bullet\text{O}_2^-$  radicals of  $\text{TiO}_2/\text{Au}$ -PDMS films under light illumination for 10 mins. g) UV-vis spectra of photocatalytic degradation of methylene blue dye over  $\text{TiO}_2/\text{Au}$ -PDMS film.

irradiating the other half, allows for the formation of a complete circuit if induced charges are produced on the irradiated half of the PDMS layer with a detectable voltage signal (the inset in Figure S12, Supporting Information). As shown in Figure 4a, when the other half is exposed to visible light, no obvious signals are generated. Together with the result that pure PDMS itself does not produce any photo-response under full spectrum (Figure S13, Supporting Information), it indicates the absence of charges on the PDMS layer when the photocatalyst  $\text{TiO}_2$  is not activated. This result also confirms that PDMS itself cannot produce charges and can only accept induced charges originating from  $\text{TiO}_2$ . Therefore, when half of the PTPC is irradiated by UV light, it shows an obvious photocurrent response, which instantaneously drops to zero when the light is off, thus affirming the dependence of the photocurrent on light. When subjected to full spectrum, the signal enhances significantly compared to UV

irradiation due to the presence of Au, which accelerates charge transport.

When a PDMS layer is incorporated atop the  $\text{TiO}_2/\text{Au}$  photocatalytic layer, induced charges emerge on the PDMS surface when  $\text{TiO}_2$  is activated.<sup>[32]</sup> PDMS possesses excellent charge preservation and poor conductivity, thereby mitigating the recombination of electron-hole pairs and prolonging the lifetime of charge carriers.<sup>[35,36]</sup> Consequently, pure PDMS shows no response when illuminated, while  $\text{TiO}_2/\text{Au}$  catalyst coated with PDMS layer exhibits a significantly higher photovoltage intensity than  $\text{TiO}_2/\text{Au}$  catalyst cast film, as measured by KPFM (Figure S14, Supporting Information; Figure 4b,c). To further verify the essential role of the PDMS layer in charge induction, the thickness of the top PDMS layer coating was optimized. Notably, an optimal thickness of 5  $\mu\text{m}$  PDMS layer coating produced the highest photovoltage intensity and achieved the optimal  $\text{H}_2$

generation rate of  $102.1 \text{ mmol m}^{-2} \text{ h}^{-1}$  (Figure 4c,d; Figure S15, Supporting Information). However, a thin PDMS ( $2 \mu\text{m}$ ) may potentially lead to charge leakage, thereby partially negating the charge induction density, while a PDMS layer of  $>5 \mu\text{m}$  increases the charge induction thickness, resulting in suboptimal thickness and diminished  $\text{H}_2$  performance.<sup>[37,38]</sup> To theoretically understand the induced charges on PDMS by underlying  $\text{TiO}_2$ , Material Studio, and COMSOL Multiphysics simulation were conducted to study the charge density on PDMS surface at both microscale and macroscale levels, respectively. There is no potential difference on PDMS when there are no charges on  $\text{TiO}_2$  (Figures S16a,S17a,d, Supporting Information), indicating PDMS itself cannot produce charge carriers, consistent with the photovoltage response and KPFM measurement. By contrast, either negative or positive charges introduced on  $\text{TiO}_2$  result in an obvious potential difference on both the top and bottom PDMS layers (Figure 4e; Figure S17b,c,e,f, Supporting Information). In addition, the thickness of PDMS layer will significantly affect the potential intensity, with a  $5 \mu\text{m}$  PDMS exhibiting higher potential induced by  $\text{TiO}_2$  (Figures S17,S18, Supporting Information).

Apart from induced charges, the reactive radicals also accumulate on the PDMS surface, evidenced by the in-situ electron paramagnetic resonance (EPR) and dye degradation reactions occurring on the PDMS surface. In Figure S19, Supporting Information and Figure 4f, compared to pure PDMS,  $\text{TiO}_2/\text{Au}$  and  $\text{TiO}_2/\text{Au}$ -PDMS samples show a strong  $\bullet\text{OH}$  signal after full spectrum irradiation for 10 min,<sup>[39]</sup> affirming oxidation reaction on the PDMS surface. Similarly,  $\text{TiO}_2/\text{Au}$ -PDMS samples also show an obvious  $\bullet\text{O}_2^-$  radicals signal, confirming the presence of the interfacial reduction and oxidation reactions on the PDMS surface.<sup>[40]</sup> Moreover, methylene blue dye degradation and Pt photo-deposition provide additional evidence of the presence of reactive radicals on the PDMS surface. This dye degradation reaction was evaluated in a customized cell showed as inset in Figure 4g and in Figure S20 (Supporting Information). After soaking the  $\text{TiO}_2/\text{Au}$ -PDMS film in the methylene blue solution in the dark for 32 h, the UV absorption shows no change, indicating that PDMS itself does not absorb methylene blue and that the PDMS structure has no physical defects that permit leakage or seepage (Figure S21, Supporting Information). In Figure 4g, a shoulder peak located at  $\approx 530 \text{ nm}$  maintains constant intensity and is ascribed to the plasmonic peak of Au, whereas the absorption peak of methylene blue dye notably decreases over 12 min, indicating successful dye degradation oxidation reaction on the PDMS surface. The degradation process typically involves both oxidation and reduction reactions to form hydroxyl radicals and superoxide anions, which can further react to degrade the dye molecules (Figure S22, Supporting Information).<sup>[41]</sup> Additionally, the presence of Pt on the  $\text{TiO}_2$ -Au PDMS film further confirms the reduction reactions on PDMS surface (Figure S23, Supporting Information). Alternative pathways for the observed redox reactions of the PTPC cannot be entirely ruled out. However, the current results indicate the presence of induced charges and reactive radicals on the PDMS surface. Drawing from the collective findings as discussed above, we postulate that the encapsulating PDMS layer serves as a reaction medium to enable interfacial redox reactions on the film surface.

To further examine the confined effect of photochemical charge transfer and photoheating, photocurrent responses of dif-

ferent films were measured. Bare photothermal material CuS showed negligible response to light. Despite CuS having excellent light absorption and narrow bandgap, these properties also adversely facilitate the recombination of photoinduced electrons and holes, limiting its use in photocatalytic redox applications.  $\text{TiO}_2/\text{Au}$  film showed a significant photocurrent signal when light was turned on and the signal dropped to zero immediately when light was switched off, indicating the strong dependence of photovoltage generation on light (Figure 5a). However, when CuS is integrated with the photoactive catalyst  $\text{TiO}_2/\text{Au}$ , the resultant PTC mixed film showed a significantly decreased photocurrent signal than that of  $\text{TiO}_2/\text{Au}$  film, indicating the interference of CuS with charge transfer of  $\text{TiO}_2/\text{Au}$ . When CuS is directly combined with  $\text{TiO}_2/\text{Au}$ , there are two scenarios that can potentially interfere with the photochemical charge transfer between cocatalyst Au and photocatalyst  $\text{TiO}_2$  (Figure 5b). Upon light excitation, both  $\text{TiO}_2$  and CuS will be activated and generate photoinduced electrons at the conduction band (CB) and holes at the valence band (VB). On one hand, the incorporation of CuS to  $\text{TiO}_2/\text{Au}$  may result in electron-hole recombination at the VB of CuS, reducing electron availability. On the other hand, based on their band structure (Figures S24,S25, Supporting Information), direct contact of  $\text{TiO}_2$  and CuS will form a Type-I heterojunction and lead to the migration of electrons and holes from  $\text{TiO}_2$  to CuS, also diminishing effective electrons for  $\text{H}_2$  production. In any case, introducing the photothermal material CuS will compromise the cocatalyst effect of Au for photochemical charge transfer-separation, making it crucial to include the PDMS spacer to avoid direct contact between the photocatalytic and photothermal layers.

The dominant role of PDMS layer was further examined by the KPFM technique. Figure 5c,d presents the topography mapping and histogram of the contact potential difference (CPD) signal of  $\text{TiO}_2/\text{Au}/\text{CuS}$  mixed film and PTPC film. With the light off, both films showed relatively low potential (Figure 5c; Figure S26, Supporting Information). However, under illumination, PTPC film produced a significantly higher signal than its counterpart without PDMS, affirming that the PDMS layer mitigates the potential interference in photochemical charge separation and photothermal effects. This finding is consistent with the corresponding  $\text{H}_2$  production activity shown in Figure 5e and Table S1 (Supporting Information). When UV light was applied, the  $\text{H}_2$  production rate of the PTPC ( $167 \text{ mmol m}^{-2} \text{ h}^{-1}$ ) was 11 times higher than that of  $\text{TiO}_2/\text{Au}/\text{CuS}$  mixed-PDMS ( $15 \text{ mmol m}^{-2} \text{ h}^{-1}$ ). In this case, UV light serves mainly as the excitation light to activate  $\text{TiO}_2$  for photocatalytic  $\text{H}_2$  evolution, therefore the sharp decline of  $\text{H}_2$  evolution activity for  $\text{TiO}_2/\text{Au}/\text{CuS}$  PTC mixed film compared to PTPC is ascribed to the shielding of active sites of  $\text{TiO}_2$  by CuS and the mutual interference of charge transfer of  $\text{TiO}_2/\text{Au}$  from photothermal material CuS. The disparity in  $\text{H}_2$  evolution becomes more significant, increasing to 12 times, under the full spectrum, suggesting that the PDMS spacer also promotes thermal management of the photothermal effect, further boosting the catalytic reaction. Moreover, substituting the photothermal material with carbon black, Ag nanoparticles, and  $\text{Ag}@\text{SiO}_2$  nanosheets, still resulted in a marked improvement in  $\text{H}_2$  production performance (Figure 5f). This illustrates the versatility of spatially decoupled film system, where photothermal material can be varied from carbon-based compounds to semiconductors and

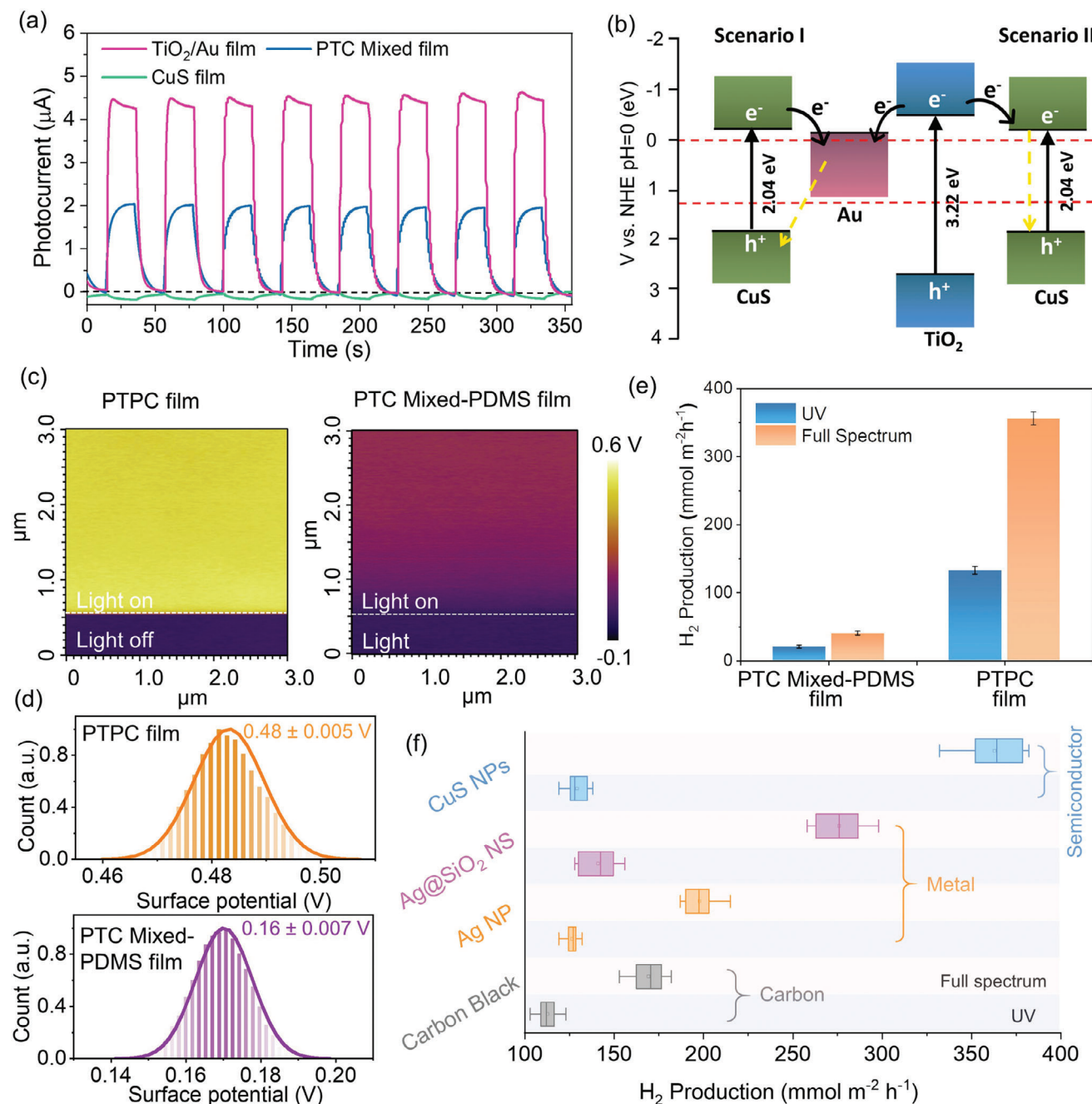


**Figure 5.** a) The photocurrent responses of CuS film, TiO<sub>2</sub>/Au/CuS PTC mixed film and TiO<sub>2</sub>/Au film. b) Schematic drawing of two possible charge transfer pathways of TiO<sub>2</sub>/Au/CuS mixed catalyst. c) Kelvin probe force microscopy (KPFM) topography mapping of PTPC film and TiO<sub>2</sub>/Au/CuS PTC mixed PDMS film in darkness and under UV light irradiation. d) Histogram of contact potential difference (CPD) signals of PTPC film and TiO<sub>2</sub>/Au/CuS PTC mixed PDMS film UV light irradiation. e) The comparison of the average H<sub>2</sub> production rate of PTPC film and TiO<sub>2</sub>/Au/CuS PTC mixed PDMS film under UV light and full spectrum irradiation. f) The hydrogen evolution rates of the PTPC film applying different photothermal materials under UV and full spectrum irradiation.

noble metals, without the concern that these materials, especially those with broadband absorption, will excessively shield the photocatalysts from the light necessary for the photogeneration process. Remarkably, the incorporation of an intermediary PDMS layer not just mitigates interference of photothermal material in photogenerated charge transfer-separation process, but also con-

fines the photothermal effect as well as allows for diverse selection of photothermal materials irrespective of band alignment compatibility.

The design of a flexible PTPC addresses some critical challenges inherent in conventional suspension systems, such as limited light penetration depth, sedimentation of the photocatalyst,

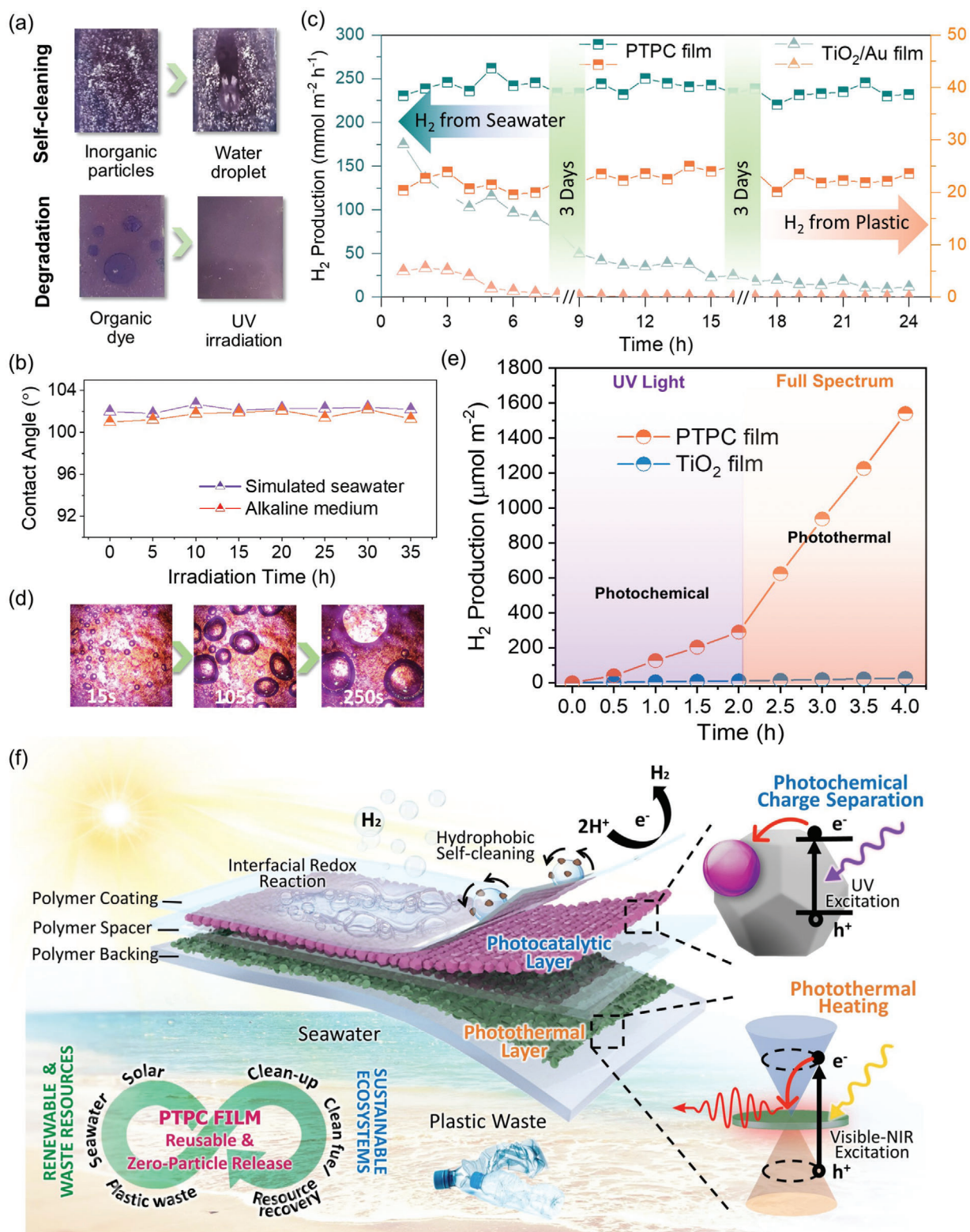


**Figure 6.** a) The self-cleaning function of the designed PTPC film for inorganic and organic contaminants. b) Contact angle of PTPC film over time in the simulated seawater and alkaline medium. c) H<sub>2</sub> production stability comparison between PTPC film and TiO<sub>2</sub>/Au film from seawater and plastic waste. d) The microscope images of hydrogen bubble evolution over time. e) Average H<sub>2</sub> production of TiO<sub>2</sub> film and PTPC film. f) The interfacial redox reactions scheme of the PTPC film.

and scalability, thus broadening the application of photocatalytic technology. Moreover, the application of PDMS layers on the top and bottom surfaces will further endow the designed PTPC with self-cleaning benefits originating from the hydrophobic characteristics of PDMS (Figure 6a). Inorganic particles on the film surface can be readily eliminated by simply rinsing with water, with particles being carried away by the water droplets. When applied to substrates containing organic dye, the PTPC film can degrade dye contaminants into inorganic substances under UV irradiation (Figure 6a).

The PDMS surface layer also serves as a protective layer for the photocatalyst and enhances stability and durability against harsh aquatic environments. When immersed in simulated seawater and alkaline medium for 35 h, the film maintains its consistent contact angle of 100° (Figure 6b). This resilience to corrosive conditions allows the PTPC to be applied in scenarios, such as H<sub>2</sub> evolution from seawater and plastic waste decomposition. Owing to the high salinity, seawater splitting is challenging as the dissolved ions in seawater may deactivate the photocatalyst or trigger undesirable side reactions.<sup>[7,42,43]</sup> As is shown in Figure 6c, the H<sub>2</sub> production rate of bare TiO<sub>2</sub>/Au film gradually declined from 175 to 42 mmol m<sup>-2</sup> h<sup>-1</sup> after 10 h testing in the seawater medium, and further dropped dramatically to 19 mmol m<sup>-2</sup> h<sup>-1</sup> after another 10 h irradiation. In contrast, flexible PTPC film maintains the average H<sub>2</sub> evolution rate at 230 mmol m<sup>-2</sup> h<sup>-1</sup> even after 24 h irradiation. Plastic waste presents a serious environmental issue due to massive usage in the past decades. Generally, plastic waste is pretreated with a highly alkaline medium to decompose plastic polymers into monomers, facilitating further decomposition and functionalization by photocatalysis. However, this highly alkaline environment will deactivate the catalyst very quickly, as evidenced by the severe decline in H<sub>2</sub> production activity of bare TiO<sub>2</sub>/Au film in Figure 6c. However, the PTPC withstands the highly alkaline medium and maintains the H<sub>2</sub> production rate at 20 mmol m<sup>-2</sup> h<sup>-1</sup> over extended test periods. Using a microscope to monitor H<sub>2</sub> bubble evolution, one can clearly observe this process over time (Figure 6d; Figure S27, Supporting Information).

Figure 6e compares the H<sub>2</sub> production of TiO<sub>2</sub> (P25) film and PTPC film, highlighting the impacts of photochemical charge transport and photothermal effects on photocatalytic H<sub>2</sub> evolution. The TiO<sub>2</sub> film, due to limited light absorption and charge separation shows low H<sub>2</sub> production activity under both UV and full spectrum and reaching up to only 25.9 μmol m<sup>-2</sup> after 4 h. In contrast, the PTPC shows H<sub>2</sub> production activity increasing steadily over time under UV, benefitting from the cocatalyst Au and photothermal component CuS. As a result, under full spectrum light, the PTPC exhibits the highest H<sub>2</sub> production activity, increasing drastically from 289.5 to 1539.8 μmol m<sup>-2</sup> in just 2 h. Additionally, the average H<sub>2</sub> evolution rate of PTPC was also much higher than those typical particulate photocatalysts reported to date (Figure S28 and Table S2, Supporting Information), demonstrating that the decoupled photoredox-photothermal pathways substantially promote the photocatalytic hydrogen evolution. The strategy of optimizing charge transfer-separation and photothermal effects can be easily realized through a layered polymer in a stacked configuration, decoupling the conflicting charge carrier pathways while providing thermal insulation and confined photoheating (Figure 6f). Additionally, the encapsulating PDMS layer acts as a passiva-

tion layer for the photocatalyst, facilitating stable catalytic performance in harsh and contaminated water environments by redirecting redox reactions on its polymeric interfacial surface. The conceptual illustration on PTPC Film: reusable and zero-particle release attributes (Figure 6f left bottom diagram) highlights the role of the polymeric layered film in advancing sustainable solutions for renewable and waste resource management. The diagram showcases its applications in transforming seawater, solar energy, and plastic waste into resource recovery, clean fuel production, and environmental clean-up outcomes. By emphasizing a zero-particle release mechanism, the PTPC Film ensures eco-friendly operations without contributing to pollution. Its reusable nature further enhances its potential to contribute significantly to sustainable ecosystems, aligning with global efforts to preserve natural resources and mitigate environmental challenges.

### 3. Conclusion

In conclusion, the development of polymeric tandem photothermal catalytic (PTPC) systems represents a pivotal innovation in film-based photothermal catalysis, particularly suited for applications in harsh environments like seawater and waste plastic media. The strategic incorporation of polymeric films both as spacer and encapsulation layers render tandem photothermal and photoredox reactions, effectively addressing the challenges of chemical stability and catalytic efficiency under adverse conditions. The PTPC system has been shown to enhance light absorption, localized heating, photothermal management, and charge transfer, while avoiding catalyst deactivation, thereby surpassing traditional suspension catalysts. Additionally, the flexibility in photocatalyst and photothermal material choice enabled by this sandwiched configuration allows for adaptation and optimization of the photothermal catalytic processes without being constrained by the requirements on band structure alignment of the involved materials. This innovation not only broadens the applicability of photothermal catalysis but also paves the way for sustainable and efficient environmental remediation and resource recovery, making it a pivotal development in the pursuit of green chemical processes.

### Supporting Information

Supporting Information is available from the Wiley Online Library or from the author.

### Acknowledgements

The authors gratefully thanked the financial support from the A\*STAR under its RIE2025 Manufacturing, Trade and Connectivity (MTC award M22K2c0081) and A\*STAR under its Individual Research Grant (IRG award M23M6c0105). Computational work was performed using resources of the National Supercomputing Centre, Singapore. The authors also express their gratitude to Dr. Xinglong Pan, Dr. Kane Jian Hong Lim, and Dr. Yuanming Zhang for assistance during the simulations and characterizations.

### Conflict of Interest

The authors declare no conflict of interest.

## Author Contributions

M.G. and T.Z. contributed equally to this work. M.G. initially conceptualized the work, prepared the film samples, and conducted the general characterizations and performance test; T.Z. performed the UV-vis and EPR characterizations, measured the performance, prepared and revised the manuscript; S.W.L.N. contributed to the preparation of film samples and conducted the electrochemical characterizations; W.L. performed the AFM characterizations and analyzed the corresponding results; G.T. performed the COMSOL simulations and analyzed the corresponding results; W.L.O. revised the manuscript and helped XRD characterizations; S.M.K. assisted in interpretation and analysis of simulation results; G.W.H. supervised the project and revised the manuscript.

## Data Availability Statement

The data that support the findings of this study are available within the article and its ESI†.

## Keywords

hydrogen production, photocatalysis, photothermal, plastic waste, seawater

Received: September 13, 2024

Revised: December 5, 2024

Published online:

- [1] Y. Qi, B. Zhang, G. Zhang, Z. Zheng, T. Xie, S. Chen, G. Ma, C. Li, K. Domen, F. Zhang, *Joule* **2024**, *8*, 193.
- [2] H. Wu, H. L. Tan, C. Y. Toe, J. Scott, L. Wang, R. Amal, Y. H. Ng, *Adv. Mater.* **2020**, *32*, 1904717.
- [3] D. Wang, M. A. Mueses, J. A. C. Marquez, F. Machuca-Martinez, I. Grcic, R. P. Muniz Moreira, G. L. Puma, *Water Res.* **2021**, *202*, 117421.
- [4] M. Gao, C. K. Peh, L. Zhu, G. Yilmaz, G. W. Ho, *Adv. Energy Mater.* **2020**, *10*, 2000925.
- [5] Q. Wang, S. Kalathil, C. Pornrungrroj, C. D. Sahm, E. Reisner, *Nat. Catal.* **2022**, *5*, 633.
- [6] W. H. Lee, C. W. Lee, G. D. Cha, B. H. Lee, J. H. Jeong, H. Park, J. Heo, M. S. Bootharaju, S. H. Sunwoo, J. H. Kim, K. H. Ahn, D. H. Kim, T. Hyeon, *Nat. Nanotechnol.* **2023**, *18*, 754.
- [7] Y. Li, H. Zhou, S. Cai, D. Prabhakaran, W. Niu, A. Large, G. Held, R. A. Taylor, X.-P. Wu, S. C. E. Tsang, *Nat. Catal.* **2024**, *7*, 77.
- [8] S. Zhang, B. Xia, Y. Qu, L. Jing, M. Jaroniec, J. Ran, S. h. Qiao, *Sci. Adv.* **2023**, *9*, adk2407.
- [9] P. Miao, J. Zhao, P. Wang, R. Shi, T. Zhang, *ACS Mater. Lett.* **2024**, *6*, 590.
- [10] X. Qiu, Y. Zhang, Y. Zhu, C. Long, L. Su, S. Liu, Z. Tang, *Adv. Mater.* **2021**, *33*, 2001731.
- [11] G. Liao, X. Tao, B. Fang, *Matter* **2022**, *5*, 377.
- [12] S. Wu, H. Yu, S. Chen, X. Quan, *ACS Catal.* **2020**, *10*, 14380.
- [13] M. Q. Yang, M. Gao, M. Hong, G. W. Ho, *Adv. Mater.* **2018**, *30*, 1802894.
- [14] L. Jiang, J. Yang, S. Zhou, H. Yu, J. Liang, W. Chu, H. Li, H. Wang, Z. Wu, X. Yuan, *Coord. Chem. Rev.* **2021**, *439*, 213947.
- [15] C. Pornrungrroj, A. B. Mohamad Annuar, Q. Wang, M. Rahaman, S. Bhattacharjee, V. Andrei, E. Reisner, *Nat. Water* **2023**, *1*, 952.
- [16] X. Zhu, H. Zong, C. J. V. Perez, H. Miao, W. Sun, Z. Yuan, S. Wang, G. Zeng, H. Xu, Z. Jiang, G. A. Ozin, *Angew. Chem., Int. Ed.* **2023**, *62*, 202218694.
- [17] S. W. L. Ng, K. J. H. Lim, M. Gao, W. Lu, T. Ghosh, M. Zhang, S. Kawi, M. Hong, G. W. Ho, *Appl. Catal., B* **2024**, *340*, 123182.
- [18] S. Fang, Y. H. Hu, *Chem. Soc. Rev.* **2022**, *51*, 3609.
- [19] G. Fu, M. Jiang, J. Liu, K. Zhang, Y. Hu, Y. Xiong, A. Tao, Z. Tie, Z. Jin, *Nano. Lett.* **2021**, *21*, 8824.
- [20] S. Guo, X. Li, J. Li, B. Wei, *Nat. Commun.* **2021**, *12*, 1343.
- [21] S. W. L. Ng, M. Gao, W. Lu, M. Hong, G. W. Ho, *Adv. Funct. Mater.* **2021**, *31*, 2104750.
- [22] Y. Xiao, Z. Fan, M. Nakabayashi, Q. Li, L. Zhou, Q. Wang, C. Li, N. Shibata, K. Domen, Y. Li, *Nat. Commun.* **2022**, *13*, 7769.
- [23] Y. Lu, H. Zhang, D. Fan, Z. Chen, X. Yang, *J. Hazard. Mater.* **2022**, *423*, 127128.
- [24] J. Zhao, P. Miao, X. Zhang, P. Wang, Z. Li, L. Z. Wu, R. Shi, T. Zhang, *Adv. Mater.* **2024**, *36*, 2400681.
- [25] M. Gao, P. K. N. Connor, G. W. Ho, *Energy Environ. Sci.* **2016**, *9*, 3151.
- [26] R. Tang, S. Zhou, L. Zhang, L. Yin, *Adv. Funct. Mater.* **2018**, *28*, 1706154.
- [27] Y. Li, H. Wang, Q. Feng, G. Zhou, Z.-S. Wang, *Energy Environ. Sci.* **2013**, *6*, 2156.
- [28] R. Yang, Y. Fan, Y. Zhang, L. Mei, R. Zhu, J. Qin, J. Hu, Z. Chen, Y. Hau Ng, D. Voiry, S. Li, Q. Lu, Q. Wang, J. C. Yu, Z. Zeng, *Angew. Chem., Int. Ed.* **2023**, *62*, 202218016.
- [29] P. Bessel, A. Niebur, D. Kranz, J. Lauth, D. Dorfs, *Small* **2023**, *19*, 2206379.
- [30] Y. Gao, W. Nie, Q. Zhu, X. Wang, S. Wang, F. Fan, C. Li, *Angew. Chem., Int. Ed.* **2020**, *59*, 18218.
- [31] X. Yu, X. Jin, X. Chen, A. Wang, J. Zhang, J. Zhang, Z. Zhao, M. Gao, L. Razzari, H. Liu, *ACS Nano* **2020**, *14*, 13876.
- [32] H.-W. Park, N. D. Huynh, W. Kim, C. Lee, Y. Nam, S. Lee, K.-B. Chung, D. Choi, *Nano Energy* **2018**, *50*, 9.
- [33] R. Chen, F. Fan, T. Dittrich, C. Li, *Chem. Soc. Rev.* **2018**, *47*, 8238.
- [34] R. Chen, Z. Ren, Y. Liang, G. Zhang, T. Dittrich, R. Liu, Y. Liu, Y. Zhao, S. Pang, H. An, C. Ni, P. Zhou, K. Han, F. Fan, C. Li, *Nature* **2022**, *610*, 296.
- [35] D. Tantraviwat, P. Buarin, S. Suntalelat, W. Sripumkhai, P. Pattamang, G. Rujijanagul, B. Inceesungvorn, *Nano Energy* **2020**, *67*, 104214.
- [36] Y. W. Kim, H. B. Lee, J. Yoon, S.-H. Park, *Nano Energy* **2022**, *95*, 107051.
- [37] X. Xie, X. Chen, C. Zhao, Y. Liu, X. Sun, C. Zhao, Z. Wen, *Nano Energy* **2021**, *79*, 105439.
- [38] M. P. Kim, C. W. Ahn, Y. Lee, K. Kim, J. Park, H. Ko, *Nano Energy* **2021**, *82*, 105697.
- [39] R. Li, Y. Weng, X. Zhou, X. Wang, Y. Mi, R. Chong, H. Han, C. Li, *Energy Environ. Sci.* **2015**, *8*, 2377.
- [40] H. Zhan, R. Zhou, P. Wang, Q. Zhou, *Proc. Natl. Acad. Sci. USA* **2023**, *120*, 2305378120.
- [41] R. Su, Y. Zhu, B. Gao, Q. Li, *Water Res.* **2024**, *251*, 121119.
- [42] J. Zhang, W. Hu, S. Cao, L. Piao, *Nano Res.* **2020**, *13*, 2313.
- [43] T. Zhang, F. Meng, Y. Cheng, N. Dewangan, G. W. Ho, S. Kawi, *Appl. Catal., B* **2021**, *286*, 119853.